Chemical pressure control of the spin-valve magnetoresistance in $La_{1.4}Sr_{1.6}Mn_2O_7$

Y. Moritomo
CIRSE and Department of Applied Physics, Nagoya University, Nagoya 464-8603, Japan
and PRESTO, JST, Chiyoda-ku, Tokyo 102, Japan

M. Itoh
Department of Applied Physics, Nagoya University, Nagoya 464-8603, Japan
(Received 21 October 1998)

Comprehensive chemical substitution effects on the magnetic and transport properties have been investigated for single crystals of $(La_{1-z}Nd_z)_{1.4}Sr_{1.6}Mn_2O_7$ with bilayer structure. In this system, the Nd-doping procedure changes the ground state from ferromagnetic (FM) to antiferromagnetic (AFM), in the latter of which the FM bilayer alternates along the *c* axis. In the Nd-doped compounds, application of an external magnetic field ($H \| c$) induces an AFM-FM metamagnetic transition. The transition accompanies a switching-like reduction of the current-perpendicular-to-plane resistivity, which can be viewed as a spin-valve magnetoresistance (MR). We have derived magnetic phase diagrams, and discuss controllability of the spin-valve MR by chemical pressure. [S0163-1829(99)03713-3]

I. INTRODUCTION

Manganese oxide with perovskitelike structure has stimulated interest because of their magnetoresistive (MR) properties;[1] they exhibit extremely large change in resistance in response to applied magnetic field. But for technological applications to magnetic memory or switching device to be viable, great improvements are needed in the field sensitivity. The so-called bilayer manganites $La_{2-2x}Sr_{1+2x}Mn_2O_7$ seems to be promising; the $x=0.4$ compound[2] shows a large MR near above the insulator-metal transition temperature $T_c=126$ K. In this compound, the MnO_2 sheets are isolated by two La(Sr)O planes, keeping the two-dimensional networks of the MnO_6 octahedra. Recently, Kimura *et al.* have reported a low-field magnetoresistance in the low-temperature phase for $La_{1.4}Sr_{1.6}Mn_2O_7$ ($x=0.3$) (Ref. 3) and enhancement of the MR under hydrostatic pressure.[4] Although exact magnetic structure as well as the origin of the MR remains controversial, this observation suggests the potentialities of the bilayer manganites for applications. To understand the origin of the low-field MR at $x=0.3$, we have performed a comprehensive study of magnetic and transport properties for $(La_{1-z}Nd_z)_{1.4}Sr_{1.6}Mn_2O_7$ with systematic variation of z ($z=0.00$, 0.03, 0.07, 0.10, 0.20, and 0.30).

Up to now, extensive studies on the lattice and magnetic structure were performed on $La_{2-2x}Sr_{1+2x}Mn_2O_7$.[5–8] In this system, the hole-doping procedure not only decreases the nominal concentration of the e_g carriers, but significantly release the static Jahn-Teller (JT) distortion of the MnO_6 octahedra:[9] averaged JT distortion Δ defined by $\langle d_{\text{Mn-}O(\text{out})}\rangle / d_{\text{Mn-}O(\text{in})}$ decreases from $\Delta=1.03$ at $x=0.3$ to 1.00 $x=0.5$. Such a variation of the JT distortion should affect the orbital character of the e_g electrons, and hence the magnetotransport properties. Moritomo *et al.*[9] have investigated the ground state properties for $(La_{1-z}Nd_z)_{2-2x}Sr_{1+2x}Mn_2O_7$ ($x=0.4$–0.5) with systematically changing z and x, and have found that the $x \geqslant 0.45$ region is dominated by a layered-type antiferromagnetic (*A*-type AFM) state. In this magnetic structure, FM MnO_2 sheet alternates along the *c* axis (intrabilayer coupling is *negative*).[7,9] Such a magnetic structure is interpreted in terms of formation of a pseudo-two-dimensional $d_{x^2-y^2}$ band, which causes the FM double-exchange interaction[10] within the MnO_2 sheet and AFM superexchange coupling between the adjacent sheets (within the bilayer). Similar *A*-type magnetic structure has been observed even in the cubic manganites[11] $R_{1-x}Sr_xMnO_3$ ($R=La_{1-z}Nd_z$) suggesting that the basic physics is similar between the bilayer and cubic manganites. Contrary to the case at $x=0.4-0.5$, the MnO_6 octahedra at $x=0.3$ significantly elongates along the *c* axis ($\Delta=1.03$), which causes stabilization of the $d_{3z^2-r^2}$ orbital as compared with the $d_{x^2-y^2}$ state. Kubota *et al.*[8] have performed a powder neutron diffraction study on the melt-grown $La_{1.4}Sr_{1.6}Mn_2O_7$; the obtained pattern at 15 K can be reproduced with FM spin structure with magnetic moment of $2.9\pm0.15\mu_B$ along the *c* axis.

Similarly to the case of hole doping, substitution of the smaller Nd^{3+} ions for La^{3+} ions (*chemical pressure*) significantly influence the magnetotransport properties of the bilayer manganites. For example, the FM metallic state at $x=0.4$ disappears when the Nd^{3+} concentration (z) exceeds 40%.[12] Such a chemical pressure effect has been ascribed to the enhanced static JT distortion and resultant change of the orbital character of the e_g electrons from $d_{x^2-y^2}$-like to $d_{3z^2-y^2}$-like. Thus, chemical pressure is a powerful technique to control the material parameters and hence the physical properties, such as the MR property.

In this paper, we systematically investigate the chemical pressure effect on the magnetotransport properties for the bilayer manganites at $x=0.3$ [$(La_{1-z}Nd_z)_{1.4}Sr_{1.6}Mn_2O_7$], which shows a large low-field MR. A part of the results at $z=0.1$ has been published as a short article:[13] we report on the AFM structure, in which ferromagnetic bilayer alternates along the *c* axis, as well as a switchinglike MR below ~ 40 K. The switchinglike MR is found to be driven by the field-

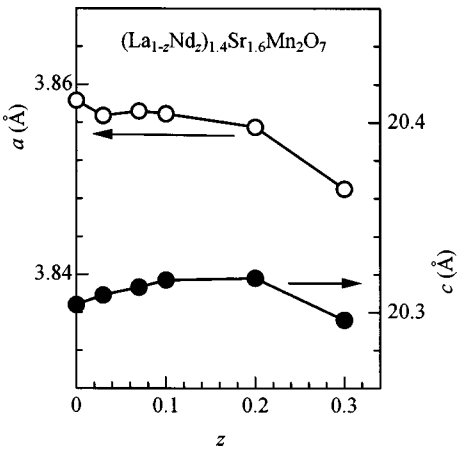

FIG. 1. Lattice constants for $(La_{1-z}Nd_z)_{1.4}Sr_{1.6}Mn_2O_7$. Open and closed circles stand for a and c.

induced AFM-FM transition, and hence is interpreted in terms of the *open and shut* natural spin valve. Here, we concentrate our attention on the chemical pressure effects on magnetic phase diagram as well as the spin-valve MR. The ratio of the current-perpendicular-to-plane (CPP) MR defined by $\rho_c(0)/\rho_c(H)$ significantly increases with increasing z though the switching field increases; the MR ratio at 0.5 T and at 40 K is $\sim$110% at $z=0.00$,$\sim$180% at $z=0.03$, $\sim$310% at $z=0.07$, and $\sim$710% at $z=0.10$. The contents of the present paper are the following. After describing the experimental details in Sec. II, we present prototypical magnetotransport properties for the FM ($z=0.0$) and AFM ($z=0.1$) compounds (Sec. III). Section IV is devoted to the chemical pressure effects on the resistivity, magnetization curve, and magnetic phase diagram. In Sec. V, we discuss controllability of the spin-valve MR by chemical pressure. A summary comes in Sec. VI.

II. EXPERIMENT

Single crystals of $(La_{1-z}Nd_z)_{1.4}Sr_{1.6}Mn_2O_7$ ($0.0 \geqslant z \geqslant 0.3$) were grown by the floating-zone method at a feeding speed of 14–20 mm/h. Stoichiometric mixture of commercial La_2O_3, Nd_2O_3, $SrCO_3$, and Mn_3O_4 powder was ground and calcined two times at 1300$-$1350 °C for 24 h. The resulting powder was pressed into a rod with a size of 5 mm$\phi\times$60 mm and sintered at 1350 °C for 24–48 h. The ingredient could be melted congruently in a flow of air. Large crystals, typically 4 mm in diameter and 20 mm in length, were obtained with two well-defined facets, which correspond to the crystallographic ab plane. Powder x-ray diffraction measurements at room temperature and Rietveld analysis[14] indicate that the crystals were nearly single phase. The crystal symmetry is tetragonal ($I4/mmm$; $Z=2$) over the whole concentration range.

The obtained lattice constants a and c are plotted in Fig. 1; open and closed circles are for a and c values, respectively. Lattice constant a gradually decreases with increase of z, while c remains nearly constant. A similar trend of the lattice constants has been observed also at $x=0.4$ (Ref. 12) and $x=0.5$.[7] Note that the c value at $x=0.3$ ($=$20.30–20.32 Å) is much larger than that of the $x=0.4$ ($=$20.15–20.16 Å),[12] reflecting the enhanced static JT distortion.[9]

For four-probe resistivity measurements, the crystal was cut into a rectangular shape, typically of $1\times1.5(ab)\times3(c)\text{mm}^3$, and electrical contacts were made with a heat-treatment-type silver paint. Special care was taken for the quality of the crystal used in the CPP-MR measurement, to avoid any extrinsic effects due to grain boundaries. In all the MR measurements, the external magnetic field is applied perpendicular to the MnO_2 ($H\|c$), or along the easy axis. The temperature dependence of magnetization was measured after cooling down to 5 K in zero field (ZFC) using a superconducting quantum interference device (SQUID) magnetometer. In the measurements of the field dependence of magnetization or resistivity, the crystal was annealed after respective field runs in the zero field at $\sim$100 K ($\gg T_N$) to eliminate any field-hysteresis effects. The upper and lower critical fields $H_{c,u}$ and $H_{c,l}$ are determined from the inflection points of the M_c-H curves in the field-increasing and -decreasing runs, respectively.

III. FERROMAGNETIC AND ANTIFERROMAGNETIC GROUND STATE

The parent $La_{1.4}Sr_{1.6}Mn_2O_7$ shows successive magnetic transitions:[8] the magnetic phase changes from paramagnetic (PM; $T\geqslant T_{N'}\sim$100 K), AFM ($T_{N'}\geqslant T\geqslant T_C\sim$70 K), to FM ($T\leqslant T_C$). In the intermediate AFM phase, the FM bilayer alternates along the c axis. The easy axis changes from the in-plane direction in the AFM phase to the out-of-plane direction in the FM state. We show in Fig. 2(a) the temperature and (b) field variation of the out-of-plane component (M_c) of magnetization for prototypical FM ($La_{1.4}Sr_{1.6}Mn_2O_7$; $z=0.0$) and AFM [$(La_{0.9}Nd_{0.1})_{1.4}Sr_{1.6}Mn_2O_7$; $z=0.1$] compounds. At $z=0.0$ (solid curve), anomalies are observed at the corresponding transition temperatures, i.e., $T_{N'}$ and T_C, in the M_c-T curve. Magnetization at 5 K ($\leqslant T_C$) readily saturates at $\mu_0 H=0.2$ T, and the saturated value ($=3.5\mu_B$) is nearly the ideal value ($=3.7\mu_B$). Such a behavior is typical of the ferromagnetic manganites.

On the other hand, the M_c-T curve at $z=0.1$ (broken curve) shows a kink structure at $T_N\sim$60 K, indicating an AFM transition. In our previous work,[13] we have measured the neutron powder pattern on the melt-grown $z=0.1$ compound, and have found that the FM bilayer alternates along the c axis in the AFM state. The estimated magnetic moment at 15 K is $3.3\pm0.05\mu_B$ along the c axis. The M_c-H curve increases gradually with field below $\sim$0.4 T, and then steeply jumps up to $2.7\mu_B$ near the ideal value, indicating an metamagnetic transition from the AFM state to FM state. The prominent field hysteresis of order of 0.1 T suggests that the transition accompanies some structural change.

Here, let us consider effects of the spin-ordering on the transport properties. The effective transfer integral t_{eff} in the double-exchange system[10] is expressed as

$$t_{\text{eff}}=t_0\cos(\theta/2), \tag{1}$$

where t_0 and θ are bare transfer integral and relative angle of the adjacent t_{2g} spins. In this model, the e_g carriers cannot

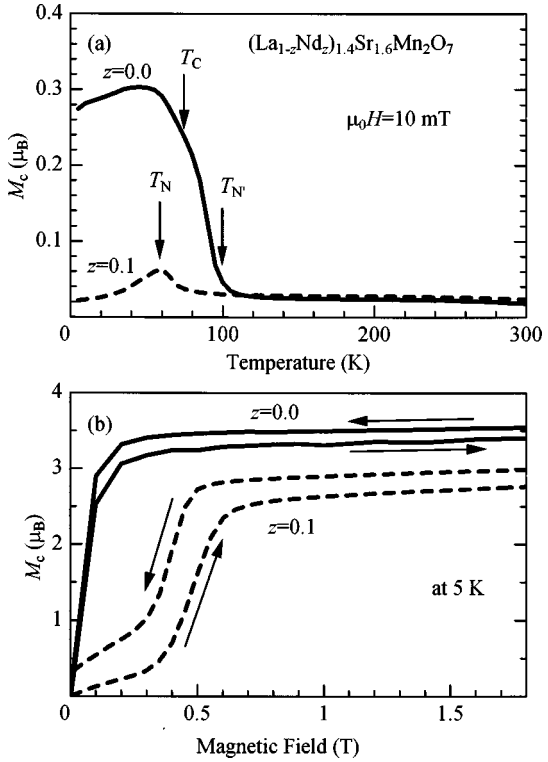

FIG. 2. (a) Temperature variation of out-of-plane component M_c of magnetization for $La_{1.4}Sr_{1.6}Mn_2O_7$ ($z=0.0$) and $(La_{0.9}Nd_{0.1})_{1.4}Sr_{1.6}Mn_2O_7$ ($z=0.1$). T_C and $T_N(T_{N'})$ means Curie and Néel temperatures, respectively. M_c was measured after cooling down to 5 K in the zero field (ZFC). (b) The M_c-T curve at 5 K for $z=0.0$ and 0.1.

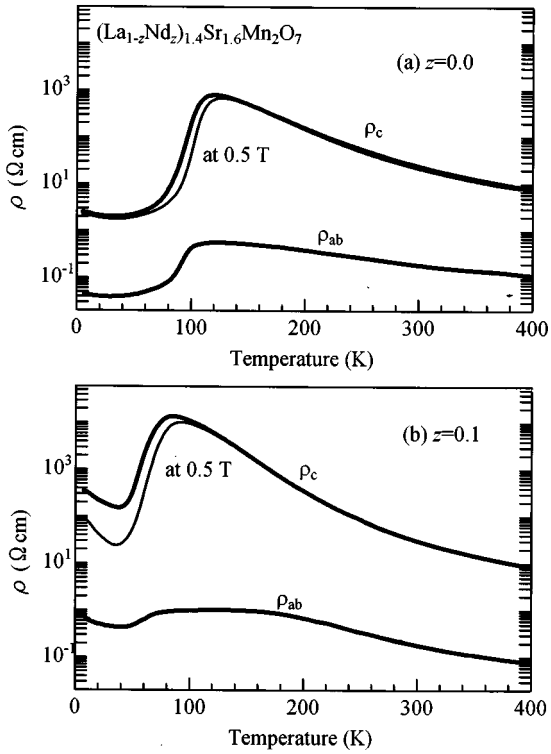

FIG. 3. Temperature variation of the in-plane ρ_{ab} and out-of-plane ρ_c components of resistivity for (a) $La_{1.4}Sr_{1.6}Mn_2O_7$ ($z=0.0$) and (b) $(La_{0.9}Nd_{0.1})_{1.4}Sr_{1.6}Mn_2O_7$ ($z=0.1$). Thin curves represent the ρ_c-T curves measured under a field of 0.5 T after cooling down to 5 K in the zero field (ZFC).

hop into the adjacent bilayers in the AFM state ($\theta=\pi$), which can be viewed as a *shut* state of the spin valve. The e_g carriers, however, can hop into the bilayers in the FM state (*open* state; $\theta=0$). In this context, the metamagnetic transition at $z=0.1$ is regarded as a transition from the *shut* state ($\leqslant$0.4 T) to *open* state ($\geqslant$0.4 T). Actually, we have observed a concomitant switchinglike MR at $z=0.1$.[13]

In Fig. 3, we show anisotropic resistivity for (a) FM ($z=0.0$) and (b) AFM ($z=1.0$) compounds together with the ρ_c-T curve measured under a field of 0.5 T (thin curve). In the FM compound ($z=0.0$; upper panel), both the components (ρ_{ab} and ρ_c) of resistivity show insulating behavior ($d\rho/dT\leqslant 0$) in the PM state, but steeply drop below $T_{N'}$ ($\sim$100 K) due to the reduced spin scattering in the spin-ordered state. Such a insulator-metal behavior of the ρ_c-T curve is consistent with the resistivity data reported by Kimura.[3] However, we cannot reproduce the metallic behavior of the ρ_{ab} component above $T_{N'}$ reported in the same literature, though we have checked several crystal ingots. Therefore, we suspect that the metallic behavior is due to some extrinsic effects, such as intergrowth of the multilayer compound inevitably introduced in the crystal growth procedure. A prominent MR (see thin curve) is observed only around the insulator-metal transition temperature ($\sim$100 K). Such a MR is ascribed to field-induced shift of the transition temperature.

A similar insulating behavior is observed at $z=0.1$ in the PM state (lower panel), though suppression of ρ_{ab} is observed below $\sim$200 K. We should emphasize that absolute value of resistivity in the spin-ordered phase is much enhanced in both components: the $\rho_{ab}(\rho_c)$ value increases from $\sim$0.04 Ω cm($\sim$2 Ω cm) at $z=0.0$ to $\sim$0.4 Ω cm ($\sim$20 Ω cm) at $z=0.1$. Such an enhancement may reflect the reduced one-electron bandwidth in the AFM state, which enhances the Anderson localization effect. Large MR behavior is observed not only around the insulator-metal transition temperature ($\sim$80 K), but in the spin-ordered phase below T_N(=60 K). The latter MR should be ascribed to the spin-valve MR, because the MR is observed only in the AFM compound.

IV. CHEMICAL PRESSURE EFFECTS

A. Magnetotransport properties

Now let us proceed to the chemical pressure effects on the magnetotransport properties. Figure 4 shows in-plane component ρ_{ab} of resistivity at various z. Downward arrows represent T_N determined by the magnetization measurements. A definite insulator-metal transition is observed at $\sim$100 K at $z=0.0$. With increase of z, the insulator-metal transition becomes blurred and the ρ_{ab} value in the AFM state increases significantly. One may notice a prominent upturn of resistivity in the AFM state, which is possibly due to the Anderson localization effect. [Note that the upturn is observed in the field-induced FM state at $z=0.1$, see Fig. 3(b).]

The chemical pressure significantly affects the metamagnetic behavior as well. Figure 5 shows a prototypical out-of-plane component M_c of magnetization curves for (a) z

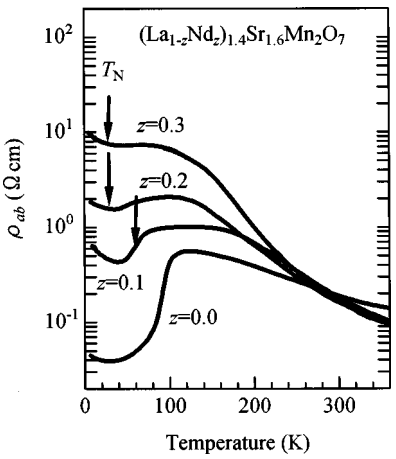

FIG. 4. Temperature variation of the in-plane ρ_{ab} components of resistivity for $(La_{1-z}Nd_z)_{1.4}Sr_{1.6}Mn_2O_7$. A downward arrow indicates the Néel temperature T_N.

$=0.03$, (b) $z=0.07$, and (c) $z=0.10$. At $z=0.10$ (lower panel), a definite AFM-FM transition is induced for at ~ 0.4 T (~ 0.3 T) at 10 K (30 K) in the field-increasing run. With further increase of temperature, the M_c-T curve shows a PM behavior (see the 70 and 100 K curve). A similar behavior is observed at $z=0.07$ (middle panel) except for slight shift of the critical field toward the low field region. At $z=0.03$ (upper panel), however, the magnetization curve increases monotonously even at the lowest temperature: the M_c value at 10 K readily saturates at $\mu_0 H=0.4$ T, and the saturated value ($=3.2\mu_B$) is nearly the ideal value. Such a behavior suggests that the ground state is FM at $z=0.03$. Observation of the spin-valve MR at $z=0.03$ (see Fig. 8), however, implies a stacking-fault-like bilayer with antiparallel spins, which works as a *shut* valve in the serially connected open-valve.

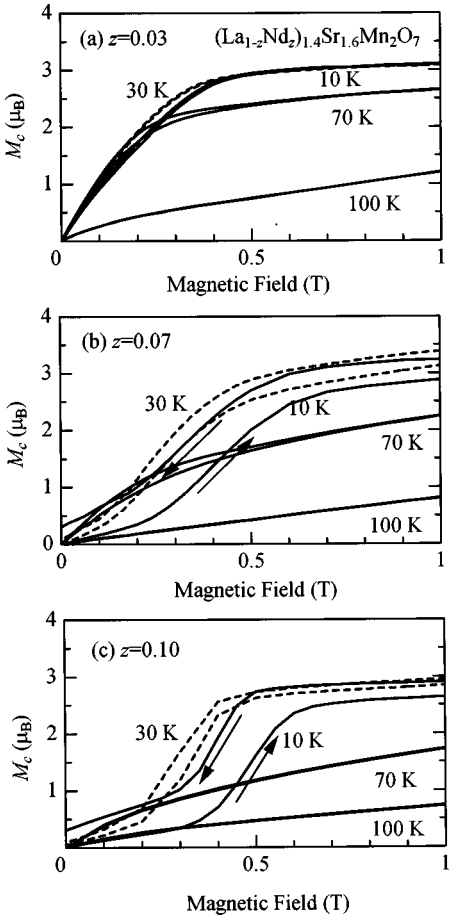

FIG. 5. Out-of-plane component M_c of magnetization curves for $(La_{1-z}Nd_z)_{1.4}Sr_{1.6}Mn_2O_7$: (a) $z=0.03$, (b) $z=0.07$, and (c) $z=0.10$.

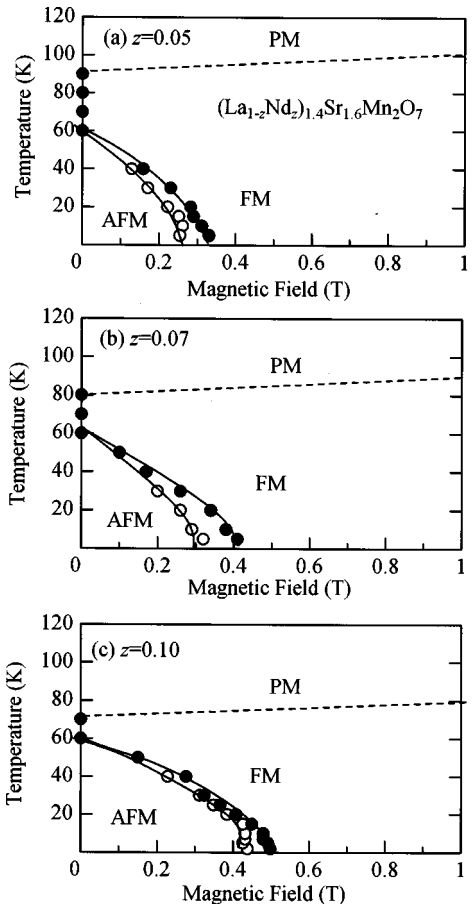

FIG. 6. Magnetic phase diagrams for $(La_{1-z}Nd_z)_{1.4}Sr_{1.6}Mn_2O_7$: (a) $z=0.05$, (b) $z=0.07$, and (c) $z=0.10$. Open and filled circles are the upper ($H_{c,u}$) and lower ($H_{c,l}$) critical fields, respectively. AFM, FM, and PM denote antiferromagnetic, ferromagnetic, and paramagnetic phases, respectively. Hatched areas stand for bistable regions.

B. Magnetic phase diagram

Using the M_c-H curves discussed above at various temperature, we have determined the magnetic phase diagrams: Fig. 6 and Fig. 7 are for low- and high-z compounds, respectively. The upper and lower critical fields $H_{c,u}$ and $H_{c,l}$ are determined from the inflection points of the M_c-H curves in the field-increasing and -decreasing runs, respectively. AFM, FM, and PM denote the antiferromagnetic, ferromagnetic, and paramagnetic states, respectively. At $z=0.05$ (upper panel in Fig. 6), the AFM state exists only in the limited region below $\mu_0 H=0.3$ T. In other words, application of external magnetic field ($\leqslant 0.3$ T; $H \| c$) forcedly aligns the t_{2g} spins, or *opens* the spin valve. Similar phase diagrams are obtained for $z=0.07$ (middle panel) and $z=0.10$ (lower

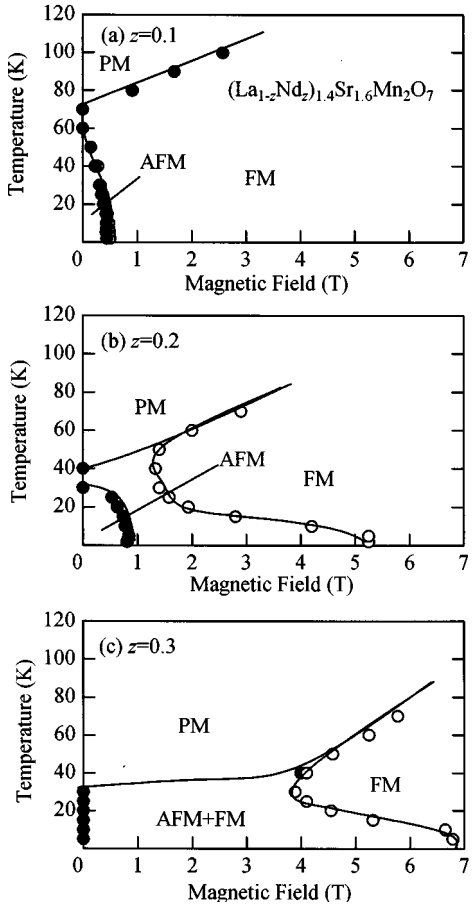

FIG. 7. Magnetic phase diagrams for $(La_{1-z}Nd_z)_{1.4}Sr_{1.6}Mn_2O_7$: (a) $z=0.1$, (b) $z=0.2$, and (c) $z=0.3$. Open and filled circles are the upper ($H_{c,u}$) and lower ($H_{c,l}$) critical fields, respectively. AFM, FM, and PM denote antiferromagnetic, ferromagnetic and paramagnetic phases, respectively. Hatched areas stand for bistable regions.

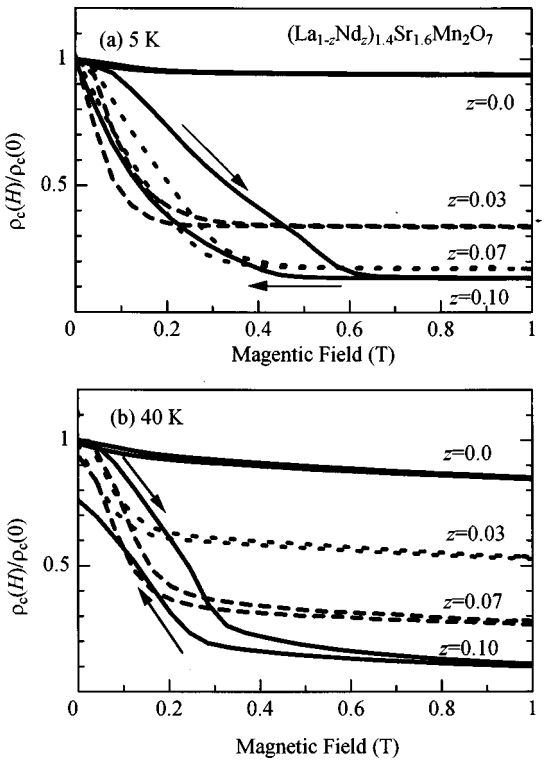

FIG. 8. Current-perpendicular-to-plane magnetoresistance (CPP-MR) for $(La_{1-z}Nd_z)_{1.4}Sr_{1.6}Mn_2O_7$ at 5 K (a) and at 40 K (b). The magnetic field was applied perpendicular to the MnO_2 sheet ($H \| c$).

panel) although the critical fields increase gradually. With further increase of z, the AFM state becomes much robust against the external magnetic field. For example, magnetic field more than 1 T is necessary to induce the AFM-FM transition at $z \geqslant 0.2$ (see middle panel of Fig. 7).

Such a strong competition between the AFM and FM state is originated in the fact that the three-dimensional magnetic structure is govern by week interbilayer exchange coupling. Note that the intrabilayer coupling is positive in the AFM state, making a sharp contrast with the *A*-type AFM state observed at $x \geqslant 0.45$.[7] In the case of $La_{1.4}Sr_{1.6}Mn_2O_7$ ($z=0.0$), the FM double-exchange interaction between the bilayer slightly overwhelms the inherent AFM superexchangelike interaction, and the FM ground state is realized. Such a subtle balance between the positive and negative interbilayer couplings can be inverted by slight structural modification induced by Nd doping, and the negative coupling dominates beyond $z=0.05$. To elucidate the microscopic origin of the interbilayer exchange coupling, detailed neutron powder diffraction measurements are now in progress. An external magnetic field cants the antiparallel t_{2g} spins in the adjacent bilayers, which switches on the interbilayer hopping of the e_g carriers. As a result, the AFM ground state becomes unstable and the AFM-FM transition is induced.

V. CONTROL OF THE SPIN-VALVE MAGNETORESISTANCE

Reflecting the AFM-FM metamagnetic transition, the CPP-MR shows a switchinglike behavior between the high-resistive (the AFM state; *shut* state) and low-resistive (the FM state; *open* state) states. Figure 8 shows a prototypical example of the CPP-MR as a function of z at 5K (a) and at 40 K (b). The CCP-MR shows a switching behavior near the critical magnetic fields for the AFM-FM transition. For example, at 40 K (lower panel) the resistance ratio for $z=0.10$ steeply decreases near the upper critical field $\mu_0 H_{c,u}$ [$=0.28$ T; see the phase diagram of Fig. 6(c)], and then becomes nearly field independent. In the field-decreasing run, the ratio begins to increase near the lower critical field $\mu_0 H_{c,l}$ ($=0.22$ T). Thus, the variation of the CPP-MR in the present system can be viewed as a spin-valve MR.

The chemical pressure significantly influences magnitude as well as field-sensitivity of the spin-valve MR. In the parent $La_{1.4}Sr_{1.6}Mn_2O_7$ ($z=0.0$), the CPP-MR at 5 K is small and shows no switchinglike behavior. With only 3% doping of the smaller Nd^{3+} ions, however, spin-valve MR appears and the magnitude of the MR increases with Nd doping: the MR ratio $[\rho_c(0)/\rho_c(H)]$ at 0.5 T and at 40 K increases from $\sim 180\%$ at $z=0.03$ to $\sim 310\%$ at $z=0.07$, to $\sim 710\%$ at $z=0.10$. Thus, the magnitude of the MR correlates with the

stability of the AFM state. The improved magnitude of the MR, however, is attained at the cost of the field sensitivity: the switching field at 40 K (lower panel) increases from ~ 0.1 T at $z=0.03$, ~ 0.2 T at $z=0.07$, and ~ 0.3 at $z=0.10$ in the field-increasing run. Accordingly, we can control the spin-valve MR properties, i.e., magnitude and field sensitivity, by chemical pressure.

Finally, let us comment on the interrelation between the present study and the pressure-enhanced low-field MR for $La_{1.4}Sr_{1.6}Mn_2O_7$. Kimura *et al.*[4] have reported enhancement of the MR under hydrostatic pressure: the MR ratio at 0.5 T and at 4.2 K increases from $\sim 400\%$ (switching field is ~ 0.1 T) at 0.0 GPa to $\sim 1600\%$ (~ 0.3 T) at 1.1 GPa. The improved magnitude of MR and reduced field sensitivity is the same trend as observed in the chemical pressure effect. This suggests that hydrostatic pressure affects the spin-valve MR also via modification of the interbilayer exchange coupling. If we choose the switching field as a crude measure for the scaling of the MR properties, the 0.0 and 1.1 GPa data correspond to the $z=0.03$ (Ref. 15) and $z=0.10$ data. Thus obtained scaling relation between the hydrostatic and chemical pressures, i.e., $z \approx 0.06P$, where P is the applied pressure in units of GPa, is close to the relation observed in the cubic manganites.[16]

VI. SUMMARY

In summary, we have systematically investigated chemical pressure effects on the magnetotransport properties, magnetic phase diagram, and spin-valve MR for $(La_{1-z}Nd_z)_{1.4}Sr_{1.6}Mn_2O_7$ with bilayer structure. In this system, the Nd doping changes the ground from ferromagnetic (*open* state of spin-valve) to antiferromagnetic (*shut* state) ones, in the latter of which FM bilayer alternates along the *c* axis. We have found close correlation between the stability of the AFM state and the spin-valve MR properties: the more stable the AFM state becomes with increase of *z*, the larger the magnitude of the MR and the lower the field-sensitivity become. Thus, we can optimize the spin-valve MR properties by chemical pressure.

ACKNOWLEDGMENTS

The authors would like to thank K. Hirota, M. Kubota, and Y. Yoshizawa for fruitful discussions. This work was supported by a Grant-In-Aid for Scientific Research from the Ministry of Education, Science, Sports and Culture, from the Precursory Research for Embryonic Science and Technology (PRESTO), the Japan Science and Technology Corporation (JST), and from the Mazda Foundation.

[1] For example, S. Jin, T. H. Tiefel, M. McCormack, R. Fastnacht, R. Ramesh, and L. H. Chen, Science **264**, 13 (1994).

[2] Y. Moritomo, A. Asamitsu, H. Kuwahara, and Y. Tokura, Nature (London) **380**, 141 (1996).

[3] T. Kimura, Y. Tomioka, H. Kuwahara, A. Asamitsu, M. Tamura, and Y. Tokura, Science **274**, 1698 (1996).

[4] T. Kimura, A. Asamitsu, Y. Tomioka, and Y. Tokura, Phys. Rev. Lett. **79**, 3720 (1997).

[5] J. F. Mitchell, D. N. Argyriou, J. D. Jorgensen, D. G. Hinks, C. D. Potter, and S. D. Bader, Phys. Rev. B **55**, 63 (1997).

[6] D. N. Argyriou, J. F. Mitchell, C. D. Potter, S. D. Bader, R. Kleb, and J. D. Jorgensen, Phys. Rev. B **55**, R11 965 (1997); D. N. Argyriou, J. F. Mitchell, J. B. Goodenough, O. Chmaissem, S. Short, and J. D. Jorgensen, Phys. Rev. Lett. **78**, 1568 (1997).

[7] K. Hirota, Y. Moritomo, H. Fujioka, M. Kubota, H. Yoshizawa, and Y. Endo, J. Phys. Soc. Jpn. **67**, 3380 (1998); Y. Moritomo, A. Nakamura, K. Ohoyama, M. Ohashi, and K. Hirota, *ibid.* (to be published).

[8] M. Kubota, H. Yoshizawa, K. Hirota, H. Fujioka, Y. Endo and Y. Moritomo, J. Phys. Chem. Solids (to be published).

[9] Y. Moritomo, Y. Maruyama, T. Akimoto, and A. Nakmura, J. Phys. Soc. Jpn. **67**, 405 (1998), and references therein.

[10] P. W. Anderson and H. Hasagawa, Phys. Rev. **100**, 675 (1955).

[11] T. Akimoto, Y. Maruyama, Y. Moritomo, A. Nakamura, K. Ohoyama, M. Ohashi, and K. Hirota, Phys. Rev. B **57**, R5594 (1998); Y. Moritomo, T. Akimoto, A. Nakamura, K. Ohoyama, and M. Ohashi, *ibid.* **58**, 5544 (1998).

[12] Y. Moritomo, Y. Maruyama, T. Akimoto, and A. Nakamura, Phys. Rev. B **56**, R7057 (1997).

[13] Y. Moritomo, K. Ohoyama, and M. Ohashi, Phys. Rev. B **59**, 157 (1999).

[14] F. Izumi, *The Rietveld Method*, edited by R. A. Young (Oxford University Press, Oxford, 1993), Chap. 13.

[15] The inconsistency between the present work and the previous one done by Kimura *et al.* is perhaps originated in slight difference of the stoichiometry between our and their crystals.

[16] Y. Moritomo, H. Kuwahara, Y. Tomioka, and Y. Tokura, Phys. Rev. B **55**, 7549 (1997).